Gridless High-Order Target Kinematic Parameter Estimation in Passive Radars—From Cross-Ambiguity Function to Zak Transform

Karol Abratkiewicz, *Member, IEEE*, and Zbigniew Gajo

***Abstract*—This article deals with practical considerations on signal processing in passive radars. First, the Zak transform is used to approximate the cross-ambiguity function (CAF) commonly applied in passive coherent location (PCL). Next, an efficient method for single-snapshot target kinematic parameter estimation is proposed. In contrast to state-of-the-art methods, the introduced technique is noniterative, numerically efficient, and has a constant computational cost. The presented approach to target kinematic parameter decomposition is compared to existing algorithms and thoroughly tested and validated in both simulations and real-life situations. A 5G-based passive radar demonstrator was used to estimate drone kinematic parameters for a representative example. As a result of signal decomposition, the maneuvering target has a narrower peak on the range-velocity (RV) map, streamlining its detection by accelerating the processing by several orders of magnitude.**

***Index Terms*—Cross-ambiguity function (CAF), high-order kinematic parameter estimation, passive radar, Zak transform.**

I. Introduction

PASSIVE radars are a kind of sensor for the range and velocity estimation of targets using a signal of opportunity, which is generally used for different purposes like communication and broadcasting [1]. However, maneuvering targets are still a challenge for radars. Rapidly varying instantaneous velocity resulting from maneuvers cannot be unambiguously determined, which, in turn, impedes unequivocal target detection. How important this problem is can be found in the extensive literature [2], [3], [4], [5], [6], [7]. In short, if the target velocity increases (or decreases) and this increment provides a notable change in the velocity, the target echo covers several range-velocity (RV) bins [8], [9]. Thus, its precise parameters cannot be clearly estimated. On the other hand, high maneuverability is a precious feature of targets (especially in military applications) like warheads, unmanned aerial vehicles, and jet fighters [10]. Thanks to this, these objects can avoid being detected by early warning and radar systems, therefore avoiding being hit and annihilated.

Received 10 June 2024; revised 15 July 2024 and 20 August 2024; accepted 21 August 2024. Date of publication 26 August 2024; date of current version 5 September 2024. *(Corresponding author: Karol Abratkiewicz.)*

The authors are with the Institute of Electronic Systems, Faculty of Electronics and Information Technology, Warsaw University of Technology, 00-665 Warsaw, Poland (e-mail: karol.abratkiewicz@pw.edu.pl).

Digital Object Identifier 10.1109/JSTARS.2024.3449392

In the literature focused on radars, this problem is usually tackled by integration time extension [11]. Next, using the range-compressed signal, the model that fits the received signal is selected in the iterative algorithm. This method is usually called the Radon-Fourier transform (RFT) and has attracted massive attention in the radar community [3], [5], [6], [12], [13]. Its main drawback is its enormous computational complexity, excluding the method's application in real-time systems [2]. Moreover, the method is parametric and requires parameter adjustment for a specific scenario. To be precise, the expected target kinematic parameters must be defined a priori and contain the actual target parameters. If the set of parameters is too wide, the processing time can be extremely long. In extreme cases, the assumed set of parameters can embrace insufficient space, leading to incorrect estimates. Another popular approach to target kinematic parameter estimation is based on multidimensional signal processing. The multidimensionality stems from modulating the received signal by factors related to kinematic parameters expected to be in the echo reflected from the moving target. The more complex the target velocity model, the higher the dimension of the result [9], [14]. The kinematic parameters of the target are determined as the maximum value of the matched filtering of the signal reflected from the object, with the reference signal modulated with subsequent values from the set. Theoretically, this kind of method seems to be a perfect solution for the problem of echo signal decomposition. In spite of this, a gory detail in practical realization is that the implementation assumes a given set of parameters to be verified. Incorrectly established borders lead to a massive computational burden or inaccurate estimation. Notwithstanding, RFT and multidimensional signal processing are a kind of maximum-likelihood estimation, but both are iterative and require searching for the optimal solution. Despite being very precise and robust against noise and clutter, these methods are still too demanding to work in real time on commercial computing platforms.

The aforementioned limitations can be circumvented when profoundly analyzing the cross-ambiguity function (CAF) and its practical implementation [15], [16], [17]. The CAF is known as an optimally matched filtering method for target detection and parameter estimation [1]. The CAF is not implemented directly in real-world applications due to the tangible computational cost [15]. Many positions in the literature do not discuss this aspect, but the CAF definition significantly differs from the practical realization of the passive radar fundamental processing

step (namely, RV map generation). This article provides deep insight into this issue. As a result, a CAF approximation is derived using the Zak transform, which, in turn, allows for an efficient high-order target kinematic parameter estimation.

The main contribution of this article can be summarized as follows.

1) A link between the theoretical considerations and the practical implementation of the signal processing pipeline in passive radars is provided. For this purpose, the RV map is practically implemented using the so-called batches algorithm (hitherto investigated as an algorithm, not a mathematically described transform), which approximates the CAF. Thus, this article is a mathematical foundation for in-depth insights into the practical aspects of passive radar signal processing with a solid theoretical background.
2) Based on the derived formulation of the passive radar signal processing considering practical aspects supported by mathematical fundamentals, a fast and gridless algorithm for high-order kinematic parameter estimation is proposed. The processing time reduction is meaningful; namely, the processing that took several hours or weeks (for a dense grid) can be accomplished in seconds. The proposed method is not as precise as maximum likelihood estimators; nevertheless, it allows for a quick assessment of target kinematic parameters for several targets simultaneously.
3) The proposed approach was experimentally validated using both simulations and a real-life 5G-based passive radar demonstrator. The estimation process was shortened from several hours to seconds.

The rest of this article is organized as follows. In Section II, the connection between the Zak transform, CAF, and Woodward's approximation is given. Next, the high-order kinematic parameter estimators are derived in Section III. In Section IV, the details of the proposed method implementation are presented. Simulations, numerical experiments, and statistical analysis are given in Section V. The discussion on computational complexity and the assumed signal model is given in Section VI. Real-life signal analysis from the 5G-based passive radar is shown in Section VII. Finally, Section VIII concludes this article.

II. From Cross-Ambiguity Function to Zak Transform

The passive radar fundamental processing step is a computation of the RV map, which, in the literature, is referred to as the CAF given as [15] and [18]

$$\Psi(t,\omega)=\int_0^{T_i} x_s(\tau)\,x_r^*(\tau-t)\,e^{-j\omega\tau}\mathrm{d}\tau \tag{1}$$

$\Psi(t,\omega)$ is a 2-D distribution of time t and Doppler angular frequency ω (for passive radar, they correspond to the bistatic range and the bistatic velocity, respectively), $x_s(t)$ is a surveillance signal, $x_r(t)$ is a reference signal, T_i is the integration time, $j=\sqrt{-1}$, and s^* denotes the complex conjugate of s. Equation (1) is typically represented as a distribution of range $t=\frac{R}{c}$ (where c is the speed of light) and velocity $\omega=2\pi v/\lambda$ (with λ as a wavelength) giving the so-called RV map. The geometry of a passive radar is sketched in Fig. 1. The blue arrow illustrates the reference signal $x_r(t)$. The red arrows present the surveillance signal $x_s(t)$, which impinges on the moving target and reaches the receiver's second antenna. The latter is a delayed and modulated copy of the direct waveform. Using (1), the delay and Doppler shift (and corresponding range and velocity) can be estimated. In this article, it is assumed that the delay of the target echo is constant during the observation, namely

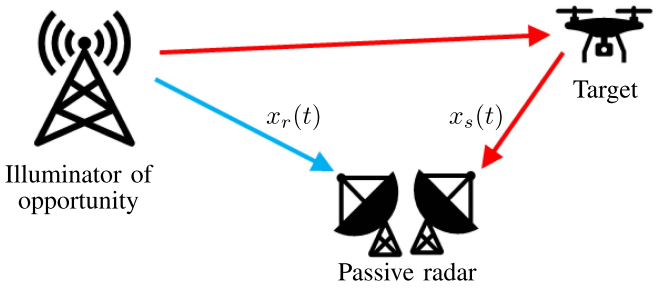

Fig. 1. Passive radar geometry.

$$\tau=\frac{R(t)}{c}\approx\text{const.} \tag{2}$$

so in the sequel of this work, $R(t)$ is simply denoted as R. Assumption (2) is reasonable for several reasons. First, it is true for short integration times when the target cannot rapidly change its position even though it maneuvers quickly. Second, the signal-to-noise ratio (SNR) has to be relatively large. When the target echo is weak, the natural way to improve its SNR is to extend the integration time, which leads to range and velocity migration. For low SNRs, especially those below 0 dB, techniques other than matched filtering typically fail. However, high-SNR cases can be accelerated by other methods, such as setting starting points for searching algorithms, and such an approach is considered in this article.

Although (1) is hardly ever implemented directly due to enormous computational cost, most of the literature positions do not mention it. Let us analyze the practical approach to RV map computation in passive radars. To do so, let $\mathcal{Z}(t,\omega)$ be the Zak transform [19], [20], which, despite being proposed for quantum mechanics, has found applications in signal processing [21], [22]. The Zak transform of the signal $x(t)$ is defined as

$$\mathcal{Z}_x(t,\omega)=\sqrt{T}\sum_{k=\infty}^{\infty}x(t+kT)e^{-j\omega kT},\quad k\in\mathbb{Z},T\in\mathbb{R}_+. \tag{3}$$

Since the scaling factor $\sqrt{T}$ does not leverage the detection performance in the radar system, for the sake of simplicity, it will be neglected in further analysis. A simplified scheme of the Zak transform can be seen in Fig. 2.

The relations between the ambiguity function and Zak transform (3) were analyzed in the literature and can be found in, e.g., [23] and [24] (especially for waveform design), suggesting that (3) can also be used for a precise description of the passive radar signal processing. The practical implementation of CAF

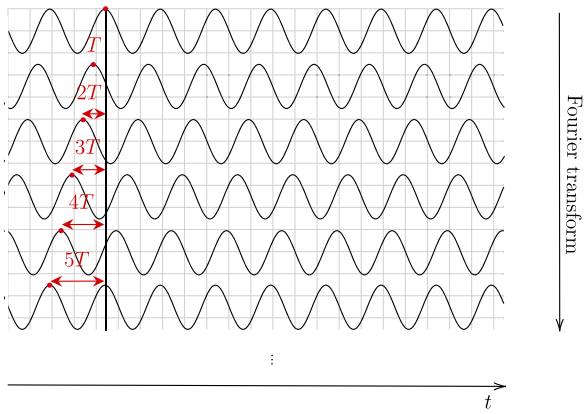

Fig. 2. Visualization of the Zak transform.

(1) proposed in the sequel of this work makes use of the cross-correlation of the surveillance signal $x_s(t)$ and the reference signal $x_r(t)$, which is defined as

$$\chi(t) = \int_{-\infty}^{\infty} x_s(\tau) x_r^*(\tau - t)\,\mathrm{d}\tau = \int_{-\infty}^{\infty} x_s(\tau + t) x_r^*(\tau)\,\mathrm{d}\tau. \tag{4}$$

In order to obtain the RV map in passive radar, the cross-correlation defined by (4) is not used directly but by dividing both signals $x_s(t)$ and $x_r(t)$ into smaller blocks (batches) and partial cross-correlations are computed on corresponding blocks using (4). Then, the windowing and the Fourier transform are performed along all blocks. The windowing operation allows for sidelobe suppression and the extraction of small echoes near strong scatterers.

To realize the practical approach described above, let us write the first cross-correlation as follows:

$$\hat{\chi}(t,0) = \int_0^{T_b} x_s(\tau) x_r^*(\tau - t)\,\mathrm{d}\tau = \int_0^{T_b} x_s(\tau + t) x_r^*(\tau)\,\mathrm{d}\tau \tag{5}$$

where T_b is the length of the signal blocks. Now, one can change the block positions by shifting them by a fixed $\zeta \in \mathbb{R}$ and write the corresponding cross-correlation as follows:

$$\hat{\chi}(t,\zeta) = \int_{\zeta}^{T_b+\zeta} x_s(\tau) x_r^*(\tau - t)\,\mathrm{d}\tau = \int_{\zeta}^{T_b+\zeta} x_s(\tau + t) x_r^*(\tau)\,\mathrm{d}\tau \tag{6}$$

or equivalently

$$\begin{aligned}\hat{\chi}(t,\zeta) &= \int_0^{T_b} x_s(\tau + \zeta) x_r^*(\tau + \zeta - t)\,\mathrm{d}\tau \\ &= \int_0^{T_b} x_s(\tau + \zeta + t) x_r^*(\tau + \zeta)\,\mathrm{d}\tau.\end{aligned} \tag{7}$$

Now, let us introduce a window in the ζ domain

$$\hat{\chi}_h(t,\zeta) = \hat{\chi}(t,\zeta) h(\zeta) \tag{8}$$

and discretize the block positions assuming $\zeta = kT$, with $k \in [-K/2, K/2)$ and fixed $T \in \mathbb{R}_+$. Next, the Fourier transform with respect to the window position is performed to obtain the RV map

$$\Phi(t,\omega) = \sum_{k=-\frac{K}{2}}^{\frac{K}{2}-1} \hat{\chi}(t,kT) h(kT) e^{-jkT\omega}. \tag{9}$$

Using (7), one can write

$$\begin{aligned}&\Phi(t,\omega) \\ &= \sum_{k=-\frac{K}{2}}^{\frac{K}{2}-1} \int_0^{T_b} x_s(\tau + kT) x_r^*(\tau + kT - t)\, h(kT) e^{-j\omega kT}\mathrm{d}\tau \\ &= \sum_{k=-\frac{K}{2}}^{\frac{K}{2}-1} \int_0^{T_b} x_s(\tau + kT + t) x_r^*(\tau + kT)\, h(kT) e^{-j\omega kT}\mathrm{d}\tau.\end{aligned} \tag{10}$$

The right-hand side of (10) can be written in a slightly different form, namely

$$\begin{aligned}&\sum_{k=-\frac{K}{2}}^{\frac{K}{2}-1} \int_0^{T_b} x_s(\tau + kT + t) x_r^*(\tau + kT)\, h(kT) e^{-j\omega kT}\mathrm{d}\tau \\ &= \sum_{k=-\frac{K}{2}}^{\frac{K}{2}-1} \int_0^{T_b} x_s(\tau + kT + t) y_r^*(\tau + kT)\mathrm{d}\tau\end{aligned} \tag{11}$$

where

$$y_r^*(\tau + kT) \overset{\text{def}}{=} x_r^*(\tau + kT) h(kT) e^{-jkT\omega}. \tag{12}$$

The right-hand side integral in (11) can be rewritten as

$$\begin{aligned}&\int_0^{T_b} x_s(\tau + kT + t) y_r^*(\tau + kT)\mathrm{d}\tau \\ &= \int_0^{T_b} x_s(\tau + kT) y_r^*(\tau + kT - t)\mathrm{d}\tau \\ &= \int_0^{T_b} x_s(\tau + kT) y_r^*(\tau + T')\mathrm{d}\tau \\ &= \int_0^{T_b} x_s(\tau + kT) x_r^*(\tau + T') h(T') e^{-j\omega T'}\mathrm{d}\tau \\ &= \int_0^{T_b} x_s(\tau + kT) x_r^*(\tau + kT - t) h(kT - t) e^{-j\omega(kT-t)}\mathrm{d}\tau\end{aligned} \tag{13}$$

where $T' = kT - t$. As a result, one can rewrite (10) as follows:

$$\begin{aligned}\Phi(t,\omega) = &\sum_{k=-\frac{K}{2}}^{\frac{K}{2}-1} \int_0^{T_b} x_s(\tau + kT) x_r^*(\tau + kT - t)\, h(kT - t) \\ &\times e^{-j\omega(kT-t)}\mathrm{d}\tau \\ = &\sum_{k=-\frac{K}{2}}^{\frac{K}{2}-1} \int_0^{T_b} x_s(\tau + kT + t) x_r^*(\tau + kT)\, h(kT) e^{-j\omega kT}\mathrm{d}\tau.\end{aligned} \tag{14}$$

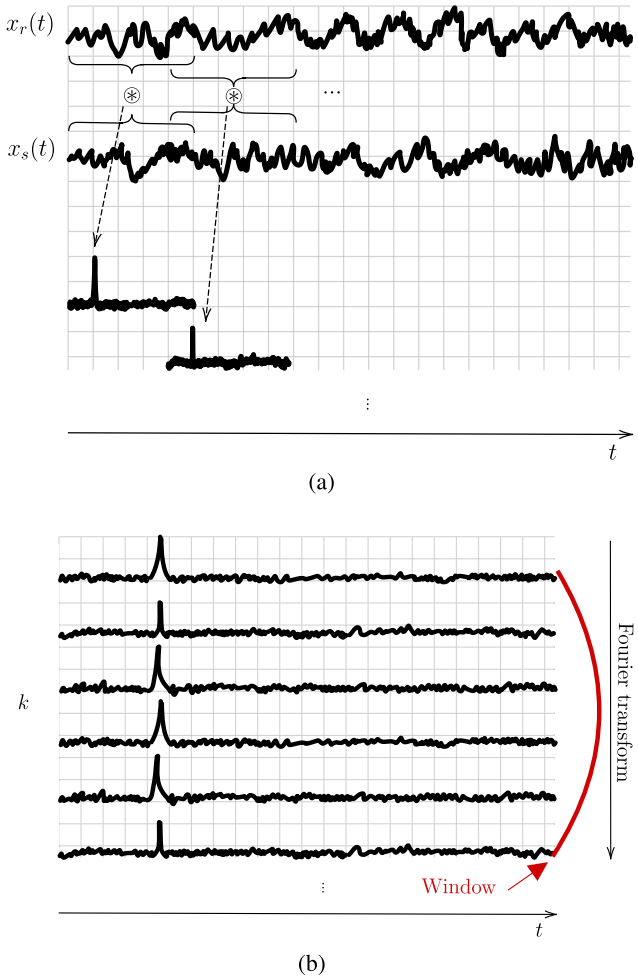

Fig. 3. Schematic idea of the RV map computation in passive radars. (a) Range profile formation through correlating signal fragments. (b) RV map computation using the Zak transform.

Now, let us focus our attention on underlining the relationship of (14) as a practical implementation of CAF with Zak transform. If we omit the window function in (14) (formally assuming that $h(t) = 1$), then for a fixed summation index k, the integrals represent cross-correlation of the reference and surveillance signals within the kth segment [see Fig. 3(a)]. Due to the assumption (2) of constant delay during observation time, these correlations are identical, and thus the summation over k, jointly with exponential factor $e^{-jkT\omega}$, can be interpreted as the Zak transform (3) (see Fig. 2). The presence of an effective window function does not change this interpretation [see Fig. 3(b)]. Thus, the notation $\mathcal{Z}^h(t,\omega)$ instead of $\Phi(t,\omega)$ in (14) is used in order to emphasize the connection of the practical implementation of CAF (1). Concluding, one can write $\Phi(t,\omega) \equiv \mathcal{Z}^h(t,\omega)$ and $\mathcal{Z}^h(t,\omega)$ is used in the sequel of this article.

The idea behind this can be seen in Fig. 3. The target echo is visualized as a peak on each range profile. The range profiles create a 2-D distribution. Dimension t is usually referred to as a *fast time*, while the second dimension (batch number) is defined as a *slow time*. The window is applied along k prior to the Fourier transform computation. The result gives the RV map.

Equation (14), especially its left-hand side, is already known in the literature devoted to radar signal processing. This form is sometimes referred to as Woodward's approximation of the CAF [15], [25], and its implementation can be found as a so-called *batches algorithm* [16]. Although it is a very efficient way to process radar data in real time, the solution is suboptimal for detection performance. It has to be stressed that (14) (or corresponding Woodward's representation of the CAF) are approximations under the premise of signal stationarity; thus, maneuvering targets are suboptimally mapped on the RV plane [this also explains the assumption on (2)]. However, this article deals with this issue, allowing for phase retrieval and high-order kinematic parameter decomposition. Also, the second alternative formulation of (14) proposed in this article allows for the tricky derivation of signal parameters while keeping the sense of the equation.

III. High-Order Target Kinematic Parameter Estimation

Let us start with a generic signal representation. The reference signal $x_r(t)$ is any waveform originating from the illuminator of opportunity. The surveillance signal $x_s(t)$ is a delayed copy of $x_r(r)$ additionally modulated in amplitude (from the radar cross-sectional characteristic) and phase (regarding the target velocity). If the target maneuvers, the bistatic velocity can be theoretically expressed as the infinity-order polynomial [9]

$$v(t) = \sum_{n=0}^{\infty} \frac{a_n(t)}{n!} t^n. \tag{15}$$

A typical assumption on a constant velocity yields

$$v(t) \approx a_1 t \tag{16}$$

where a_1 is the constant velocity (the initial phase was neglected). However, this assumption can no longer hold true for maneuvering targets, leading to a blur of the RV map and limited possibility of target detection [9], [10]. In the next part of this article, (16) is extended to a higher order polynomial. The surveillance signal can be expressed as

$$x_s(t) = A_x(t) e^{j\phi_x(t)} x_r\left(t - \frac{R}{c}\right) = x_e(t) x_r\left(t - \frac{R}{c}\right) \tag{17}$$

where $x_r(t - \frac{R}{c})$ is the reference signal delayed according to R, and $x_e(t)$ is the factor related to target maneuvers. Differentiating (17) with respect to time yields

$$\frac{\mathrm{d}x_s(t)}{\mathrm{d}t} = \frac{\mathrm{d}x_r\left(t - \frac{R}{c}\right)}{\mathrm{d}t} x_e(t) + x_r\left(t - \frac{R}{c}\right) \frac{\mathrm{d}x_e(t)}{\mathrm{d}t}. \tag{18}$$

For $\mathcal{Z}^h(t,\omega)$, its partial derivative with respect to t reads as

$$\frac{\partial \mathcal{Z}^h(t,\omega)}{\partial t} = \sum_{k=-\frac{K}{2}}^{\frac{K}{2}-1} \int_0^{T_b} x_s(\tau + kT) \times \frac{\partial x_r^*\left(\tau + kT - t\right) h(kT - t) e^{-j\omega(kT-t)}}{\partial t} \mathrm{d}\tau$$

$$= \sum_{k=-\frac{K}{2}}^{\frac{K}{2}-1} \int_0^{T_b} \frac{\partial x_s(\tau+kT+t)}{\partial t} x_r^*(\tau+kT)\, h(kT) e^{-j\omega kT} \mathrm{d}\tau. \tag{19}$$

Substituting (18) into the right-hand side of (19) leads to

$$\begin{aligned}
&-\mathcal{Z}^{\mathcal{D}h}(t,\omega) \\
&+ j\omega \sum_{k=-\frac{K}{2}}^{\frac{K}{2}-1} \int_0^{T_b} x_s(\tau+kT) x_r^*(\tau+kT-t)\, h(kT-t) \\
&\times e^{-j\omega(kT-t)} \mathrm{d}\tau \\
&+ \sum_{k=-\frac{K}{2}}^{\frac{K}{2}-1} \int_0^{T_b} x_s(\tau+kT) \frac{\partial x_r^*(\tau+kT-t)}{\partial t} h(kT-t) \\
&\times e^{-j\omega(kT-t)} \mathrm{d}\tau \\
&= \sum_{k=-\frac{K}{2}}^{\frac{K}{2}-1} \int_0^{T_b} \left[\frac{\partial x_r\left(\tau+kT+t-\frac{R}{c}\right)}{\partial t} x_e(\tau+kT+t) \right. \\
&\left. + x_r\left(\tau+kT+t-\frac{R}{c}\right) \frac{\partial x_e(\tau+kT+t)}{\partial t} \right] x_r^*(\tau+kT) \\
&\times h(kT) e^{-j\omega kT} \mathrm{d}\tau
\end{aligned} \tag{20}$$

where $\mathcal{Z}^{\mathcal{D}h}(t,\omega)$ is the transform $\mathcal{Z}^{h}(t,\omega)$ computed using the window derivative so that $\mathcal{D}h = \frac{\mathrm{d}h(t)}{\mathrm{d}t}$. Next

$$\begin{aligned}
&j\omega\mathcal{Z}^{h}(t,\omega) - \mathcal{Z}^{\mathcal{D}h}(t,\omega) \\
&+ \sum_{k=-\frac{K}{2}}^{\frac{K}{2}-1} \int_0^{T_b} x_s(\tau+kT) \frac{\partial x_r^*(\tau+kT-t)}{\partial t} h(kT-t) \\
&\times e^{-j\omega(kT-t)} \mathrm{d}\tau \\
&= \sum_{k=-\frac{K}{2}}^{\frac{K}{2}-1} \int_0^{T_b} \frac{\partial x_r\left(\tau+kT+t-\frac{R}{c}\right)}{\partial t} x_e(\tau+kT+t) \\
&\times x_r^*(\tau+kT) h(kT) e^{-j\omega kT} \mathrm{d}\tau \\
&+ \sum_{k=-\frac{K}{2}}^{\frac{K}{2}-1} \int_0^{T_b} x_r\left(\tau+kT+t-\frac{R}{c}\right) \frac{\partial x_e(\tau+kT+t)}{\partial t} \\
&\times x_r^*(\tau+kT) h(kT) e^{-j\omega kT} \mathrm{d}\tau
\end{aligned} \tag{21}$$

which can be further expressed by (22), shown at the bottom of this page (remembering that $x_s(t) = x_e(t) x_r(t-\frac{R}{c})$). Since $A = B$, one has

$$\begin{aligned}
&\mathcal{Z}^{\mathcal{D}h}(t,\omega) = j\omega\mathcal{Z}^{h}(t,\omega) \\
&- \sum_{k=-\frac{K}{2}}^{\frac{K}{2}-1} \int_0^{T_b} x_r\left(\tau+kT+t-\frac{R}{c}\right) \frac{\partial x_e(\tau+kT+t)}{\partial t} \\
&\times x_r^*(\tau+kT) h(kT) e^{-j\omega kT} \mathrm{d}\tau.
\end{aligned} \tag{23}$$

At this point, let us define the generic echo signal model as

$$x_e(t) = A_x(t) e^{j\phi_x(t)}. \tag{24}$$

Let us define the echo signal using the Taylor expansion in t close to τ. Doing so, one has [26]

$$\log\left(A_x(t)\right) = \sum_{n=0}^{N} \frac{\left(\log A_x\right)^{(n)}(\tau)}{n!} (t-\tau)^n \tag{25}$$

and

$$\phi_x(t) = \sum_{n=0}^{N} \frac{\phi_x^{(n)}(\tau)}{n!} (t-\tau)^n \tag{26}$$

where $s^{(n)}$ denotes the nth order derivative of s with respect to time. Thus, substituting (25) and (26) into (23) gives

$$\begin{aligned}
\mathcal{Z}^{\mathcal{D}h}(t,\omega) = j\omega\mathcal{Z}^{h}(t,\omega) - \sum_{k=-\frac{K}{2}}^{\frac{K}{2}-1} \int_0^{T_b} x_r\left(\tau+kT+t-\frac{R}{c}\right) \\
\times \frac{\partial}{\partial t} \exp\left(\sum_{n=0}^{N} \frac{\left(\log A_x\right)^{(n)}(\tau)}{n!} (t+kT)^n \right.
\end{aligned}$$

$$\begin{aligned}
j\omega\mathcal{Z}^{h}(t,\omega) - \mathcal{Z}^{\mathcal{D}h}(t,\omega) + \overbrace{\sum_{k=-\frac{K}{2}}^{\frac{K}{2}-1} \int_0^{T_b} x_r\left(\tau+kT-\frac{R}{c}\right) x_e(\tau+kT) \frac{\partial x_r^*(\tau+kT-t)}{\partial t} h(kT-t) e^{-j\omega(kT-t)} \mathrm{d}\tau}^{A} \\
= \underbrace{\sum_{k=-\frac{K}{2}}^{\frac{K}{2}-1} \int_0^{T_b} \frac{\partial x_r\left(\tau+kT+t-\frac{R}{c}\right)}{\partial t} x_e(\tau+kT+t) x_r^*(\tau+kT) h(kT) e^{-j\omega kT} \mathrm{d}\tau}_{B} \\
+ \sum_{k=-\frac{K}{2}}^{\frac{K}{2}-1} \int_0^{T_b} x_r\left(\tau+kT+t-\frac{R}{c}\right) \frac{\partial x_e(\tau+kT+t)}{\partial t} x_r^*(\tau+kT) h(kT) e^{-j\omega kT} \mathrm{d}\tau.
\end{aligned} \tag{22}$$

$$+j\sum_{n=0}^{N}\frac{\phi_x^{(n)}(\tau)}{n!}(t+kT)^n\Bigg)x_r^*(\tau+kT)h(kT)e^{-j\omega kT}\mathrm{d}\tau. \tag{27}$$

Let us assume that the amplitude and the phase of the echo signal (24) are defined by the fourth-order polynomial so that $N=4$, so its Gaussian-based formula reads as $A_x(t)=$

$$\mathcal{A}_x\cdot\exp\left(-\frac{(t-t_x)^2}{2T_x^2}-\Delta_x\frac{(t-t_x)^3}{3T_x^2}-\Sigma_x\frac{(t-t_x)^4}{4T_x^2}\right) \tag{28}$$

$\mathcal{A}_x$ is the constant envelope, t_x is the time shift, T_x is the duration, and components $-\frac{(t-t_x)^2}{2T_x^2}$, $-\Delta_x\frac{(t-t_x)^3}{3T_x^2}$, and $-\Sigma_x\frac{(t-t_x)^4}{4T_x^2}$ are responsible for the second, third, and fourth-order amplitude modulation component, respectively. The phase can then be described as

$$\phi_x(t)=\varphi_x+\omega_x t+\alpha_x t^2/2+\beta_x t^3/3+\gamma_x t^4/4 \tag{29}$$

where the initial phase is denoted as $\varphi_x=2\pi a_0$, $\omega_x=2\pi a_1/\lambda$, $\alpha_x=2\pi a_2/\lambda$, $\beta_x=2\pi a_3/\lambda$, and $\gamma_x=2\pi a_4/\lambda$ are the first, second, third, and fourth-order modulation terms responsible for target velocity, acceleration, jerk, and snap, respectively. Including (28) and (29) in the signal model, its derivative is as follows:

$$\frac{\mathrm{d}x_e(t)}{\mathrm{d}t}=\left(p_x t^3+q_x t^2+r_x t+s_x\right)x_e(t) \tag{30}$$

where

$$p_x=\frac{-\Sigma_x}{T_x^2}+j\gamma_x, \tag{31}$$

$$q_x=\frac{-\Delta_x+3\Sigma_x t_x}{T_x^2}+j\beta_x \tag{32}$$

$$r_x=-\frac{1-2\Delta_x t_x+3\Sigma_x t_x^2}{T_x^2}+j\alpha_x \tag{33}$$

$$s_x=\frac{t_x-\Delta_x t_x^2+\Sigma_x t_x^3}{T_x^2}+j\omega_x. \tag{34}$$

Substituting (30) into (27) and grouping the formula, one has

$$\begin{aligned}\mathcal{Z}^{\mathcal{D}h}(t,\omega)=&-p_x\mathcal{Z}^{\mathcal{T}^3h}(t,\omega)\\&-(3p_xt+q_x)\mathcal{Z}^{\mathcal{T}^2h}(t,\omega)\\&-(3p_xt^2+2q_xt+r_x)\mathcal{Z}^{\mathcal{T}h}(t,\omega)\\&-(p_xt^3+q_xt^2+r_xt+s_x-j\omega)\mathcal{Z}^{h}(t,\omega)\end{aligned} \tag{35}$$

where $\mathcal{T}^n h=t^n h(t)$. To estimate parameters $a_0\ldots a_4$, let us build a linear system allowing for derivations of target kinematic parameters. Differentiating (35) once with respect to ω yields

$$\begin{aligned}\mathcal{Z}^{\mathcal{D}\mathcal{T}h}(t,\omega)+\mathcal{Z}^{h}(t,\omega)=&-p_x\mathcal{Z}^{\mathcal{T}^4h}(t,\omega)\\&-(3p_xt+q_x)\mathcal{Z}^{\mathcal{T}^3h}(t,\omega)\\&-(3p_xt^2+2q_xt+r_x)\mathcal{Z}^{\mathcal{T}^2h}(t,\omega)\\&-(p_xt^3+q_xt^2+r_xt+s_x-j\omega)\mathcal{Z}^{\mathcal{T}h}(t,\omega).\end{aligned} \tag{36}$$

In general, the $(n-3)$th-order derivative (for $n\geq 4$) of (35) with respect to ω can be obtained as

$$\begin{aligned}\mathcal{Z}^{\mathcal{T}^{n-3}\mathcal{D}}(t,\omega)+(n-4)\mathcal{Z}^{\mathcal{T}^{n-3}}(t,\omega)=&-p_x\mathcal{Z}^{\mathcal{T}^n}(t,\omega)\\&-(3p_xt+q_x)\mathcal{Z}^{\mathcal{T}^{n-1}}(t,\omega)\\&-(3p_xt^2+2q_xt+r_x)\mathcal{Z}^{\mathcal{T}^{n-2}}(t,\omega)\\&-(p_xt^3+q_xt^2+r_xt+s_x-j\omega)\mathcal{Z}^{\mathcal{T}^{n-3}}(t,\omega)\end{aligned} \tag{37}$$

where $\mathcal{Z}^{\mathcal{T}^n\mathcal{D}}(t,\omega)$ is a combined window derivative multiplied by the nth order time ramp. Using (35), (36), and the two next derivatives of (36) with respect to ω according to (37), the following linear system can be written (to simplify the notation, (t,ω) was omitted):

$$\begin{bmatrix}\mathcal{Z}^{\mathcal{T}^3h}&\mathcal{Z}^{\mathcal{T}^2h}&\mathcal{Z}^{\mathcal{T}h}&\mathcal{Z}^{h}\\\mathcal{Z}^{\mathcal{T}^4h}&\mathcal{Z}^{\mathcal{T}^3h}&\mathcal{Z}^{\mathcal{T}^2h}&\mathcal{Z}^{\mathcal{T}h}\\\mathcal{Z}^{\mathcal{T}^5h}&\mathcal{Z}^{\mathcal{T}^4h}&\mathcal{Z}^{\mathcal{T}^3h}&\mathcal{Z}^{\mathcal{T}^2h}\\\mathcal{Z}^{\mathcal{T}^6h}&\mathcal{Z}^{\mathcal{T}^5h}&\mathcal{Z}^{\mathcal{T}^4h}&\mathcal{Z}^{\mathcal{T}^3h}\end{bmatrix}$$

$$\times\begin{bmatrix}-p_xt^3-q_xt^2-r_xt-s_x+j\omega\\-3p_xt^2-2q_xt-r_x\\-3p_xt-q_x\\-p_x\end{bmatrix}=\begin{bmatrix}\mathcal{Z}^{\mathcal{D}h}\\\mathcal{Z}^{\mathcal{D}\mathcal{T}h}+\mathcal{Z}^{h}\\\mathcal{Z}^{\mathcal{D}\mathcal{T}^2h}+2\mathcal{Z}^{\mathcal{T}h}\\\mathcal{Z}^{\mathcal{D}\mathcal{T}^3h}+3\mathcal{Z}^{\mathcal{T}^2h}\end{bmatrix} \tag{38}$$

which leads to (if the inverse matrix can be obtained)

$$\begin{bmatrix}v_1\\v_2\\v_3\\v_4\end{bmatrix}=\begin{bmatrix}-p_xt^3-q_xt^2-r_xt-s_x+j\omega\\-3p_xt^2-2q_xt-r_x\\-3p_xt-q_x\\-p_x\end{bmatrix}=$$

$$\begin{bmatrix}\mathcal{Z}^{\mathcal{T}^3h}&\mathcal{Z}^{\mathcal{T}^2h}&\mathcal{Z}^{\mathcal{T}h}&\mathcal{Z}^{h}\\\mathcal{Z}^{\mathcal{T}^4h}&\mathcal{Z}^{\mathcal{T}^3h}&\mathcal{Z}^{\mathcal{T}^2h}&\mathcal{Z}^{\mathcal{T}h}\\\mathcal{Z}^{\mathcal{T}^5h}&\mathcal{Z}^{\mathcal{T}^4h}&\mathcal{Z}^{\mathcal{T}^3h}&\mathcal{Z}^{\mathcal{T}^2h}\\\mathcal{Z}^{\mathcal{T}^6h}&\mathcal{Z}^{\mathcal{T}^5h}&\mathcal{Z}^{\mathcal{T}^4h}&\mathcal{Z}^{\mathcal{T}^3h}\end{bmatrix}^{-1}\begin{bmatrix}\mathcal{Z}^{\mathcal{D}h}\\\mathcal{Z}^{\mathcal{D}\mathcal{T}h}+\mathcal{Z}^{h}\\\mathcal{Z}^{\mathcal{D}\mathcal{T}^2h}+2\mathcal{Z}^{\mathcal{T}h}\\\mathcal{Z}^{\mathcal{D}\mathcal{T}^3h}+3\mathcal{Z}^{\mathcal{T}^2h}\end{bmatrix}. \tag{39}$$

Hence, the following estimators can be obtained recursively:

$$\hat{p}_x=-v_4 \tag{40}$$

$$\hat{q}_x=-2\hat{p}_x\hat{t}(t,\omega)-v_3 \tag{41}$$

$$\hat{r}_x=-3\hat{p}_x[\hat{t}(t,\omega)]^2-2\hat{q}_x\hat{t}(t,\omega)-v_2 \tag{42}$$

$$\hat{s}_x=-\hat{p}_x[\hat{t}(t,\omega)]^3-\hat{q}_x[\hat{t}(t,\omega)]^2-\hat{r}_x\hat{t}(t,\omega)-v_1+j\omega \tag{43}$$

where

$$\hat{t}(t,\omega)=\frac{\mathcal{Z}^{\mathcal{T}h}(t,\omega)}{\mathcal{Z}^{h}(t,\omega)}. \tag{44}$$

See Appendix for derivations of (44). Estimated factors can be transformed on m/s^n by taking the imaginary part $\Im$ and scaling by $\lambda/2\pi$ as follows:

$$\hat{a}_4(t,\omega) = \hat{\gamma}_x(t,\omega)\cdot\lambda/2\pi = \Im(\hat{p}_x)\cdot\lambda/2\pi \text{ m/s}^4 \quad (45)$$

$$\hat{a}_3(t,\omega) = \hat{\beta}_x(t,\omega)\cdot\lambda/2\pi = \Im(\hat{q}_x)\cdot\lambda/2\pi \text{ m/s}^3 \quad (46)$$

$$\hat{a}_2(t,\omega) = \hat{\alpha}_x(t,\omega)\cdot\lambda/2\pi = \Im(\hat{r}_x)\cdot\lambda/2\pi \text{ m/s}^2 \quad (47)$$

$$\hat{a}_1(t,\omega) = \hat{\omega}_x(t,\omega)\cdot\lambda/2\pi = \Im(\hat{s}_x)\cdot\lambda/2\pi \text{ m/s}. \quad (48)$$

The signal must be decomposed to fully characterize a moving target since higher order terms affect lower-order ones. From (18), we see that p_x, q_x, and r_x bias the signal velocity if any of them is nonzero. The next section describes the algorithm for target kinematic parameter decomposition.

IV. Implementation

The estimation process proposed in this article amounts to the computation of 11 RV maps with different windows and solving the linear system given by (39). The main pros of this method in terms of implementation in real-life systems are as follows.

1) Constant complexity—one always needs the same number of RV maps for the solution of (39), making the proposed technique versatile.
2) Analysis windows are given a priori—RV maps used in (39) differ in the analysis windows (derivative of the window $\mathcal{D}^n h$ or the window multiplied by the time ramp $\mathcal{T}^n h$); thus, they can be stored in memory without the need to compute the coefficients every time.
3) Nonparametricity—the method surpasses other state-of-the-art techniques [5], [9] as it does not work under a prerequisite of a given grid and its boundaries; thus, it cannot happen that the estimated value is off-grid or out of the analyzed range.
4) Noniterativity—methods known in the literature are iterative [5], [9] and need the computation of a given function (RV map or range-compressed signal) for each value from the grid, which is extremely time-consuming and obstructs real-time systems. Additionally, the iterations are nested for several kinematic parameters, leading to a huge computational complexity.

As mentioned in the previous section, a full parametrization of the target requires the gradual decomposition of the echo signal from the highest considered polynomial order to the lowest one, which stems from (18). Since this article assumes the fourth-order polynomial echo signal, further considerations are conducted under this prerequisite. However, the method can be extended to any order of the kinematic parameter.

Algorithm 1 presents the procedure of kinematic parameter estimation using MATLAB pseudocode. In short, the algorithm comes down to several main steps.

1) Compute RV maps with different windows and estimate parameter $\hat{a}_4(t,\omega)$.
2) For a given target, progressively decompose its parameters by demodulating the signal beginning with the highest-order polynomial component.

Algorithm 1: Pseudocode for Target Echo Signal Decomposition.

```
Input:
    x_r % Reference signal vector
    x_s % Surveillance signal vector
Define:
    fs % Sampling rate
    fc % Carrier frequency
    max_t % Maximum time
    max_omega % Maximum frequency
    K % Number of batches
    kin_params % Kinematic parameters
    t % Time vector
    L % Signal length
    lambda % Wavelength
Initialize arrays:
    X_r(max_t, K) % For x_r signal
    X_s(max_t, K) % For x_s signal
    RC(max_t, K) % For range
    compression
    kin_params = [0,0,0,0]
    t=((L/2-1):L/2)./fs
    lambda=c/fc
Generate windows:
    h, ht, ht2, ht3, ht4, ht5, ht6,
dh,
    dht, dht2, dht3 % Windows for
(39)
Divide signal x_r into overlapping batches:
    X_r % Reference signal 2-D matrix
for i = 4 : 1 do
  Divide signal x_s into overlapping batches:
    X_s % Surveillance signal 2D
matrix
  Correlate X_r and X_s for each k ∈ (−K/2, K/2]:
    RC =
ifft(fft(conj(X_r)).*fft(X_s))
    % Range compression
  Compute RV maps with each window:
    Zh, Zht, Zht2, Zht3, Zht4, Zht5,
    Zht6, Zdh, Zdht, Zdht2, Zdht3
  Solve (39) obtaining a_4...a_1
  Scale the result to m/s^n
  Assign kin_params(i)=a_i
  Demodulate x_s as
    mod=kin_params(i)/i/lambda
    x_s=x_s.*exp(−1j*2*pi*t.^ i*mod)
end for
Return:
    Zh % Range-velocity map
    kin_params % Target kinematic
params
```

3) Repeat points 1. and 2. for the assumed polynomial order.

The implementation can be performed efficiently thanks to the fast Fourier transform (FFT) for correlating signals and velocity estimation. Also, the window and its different variants are fixed for the whole processing and can be computed only once. In

TABLE I
PARAMETERS OF THE SIMULATION

	Target 1	Target 2	Target 3
Range [m]	100	50	150
Velocity [m/s]	5	−10	10
Acceleration [m/s^2]	0.5	−0.5	−1
Jerk [m/s^3]	20	50	−10
Snap [m/s^4]	150	−100	100

this way, the results presented in the sequel of this article were obtained.

V. SIMULATIONS

All of the simulation results presented in the further part of this article were obtained using a desktop computer with the MATLAB 2023b environment, CPU Intel i9-13900KF 3 GHz, 64 GB DDR4, SSD drive, and Windows 10.

A. Example of Method's Usability

Let us analyze a three-target scenario for a passive radar. The simulation parameters were as follows: carrier frequency $f_c = 3.44$ GHz, sampling rate $f_s = 50$ MSa/s, and integration time $T_i = 250$ ms. The illuminating signal was a noise waveform imitating an orthogonal frequency division multiplexing (OFDM). The targets' parameters are itemized in Table I.The targets' signal energy before integration was assumed to be 100 dB weaker than the reference one (the echo from each target was the same in terms of energy). However, comprising the integration gain given as

$$G_i = BT_i \tag{49}$$

where B is the signal bandwidth, the SNR was almost 42 dB. This assumption aligns with the experiments presented in the next section and with the general concept for maneuvering target detection using short integration time in single-snapshot processing.

The typical processing is based on correlating signal batches, and spectral analysis was carried out. Next, using the proposed method, target parameters were estimated. This example focuses on estimating targets' snap due to the limited scope of the article. Further parameters are estimated and shown in the sequel of this article. The aim of the results shown in Fig. 4 is to visualize the principle of operation of the proposed method. First, Fig. 4(a) presents the RV map with apparent targets with range and velocity related to Table I. Next, Fig. 4(b) demonstrates the outcome of target snap estimation. As can be observed, the estimate is given for the whole distribution, allowing for each observed target parametrization. For the sake of clarity, the results of the target parameter estimation for acceleration, jerk, and snap are illustrated in the form of saturated distribution, where the alpha channel of the figure corresponds to the energy in the RV map, which is delineated in Fig. 4(c). The advantage of such data visualization is that only the influencing targets are visible while all the backgrounds with significantly lower energy are in white. However, it has to be kept in mind that the saturated distribution does not mean that the parameters are not estimated

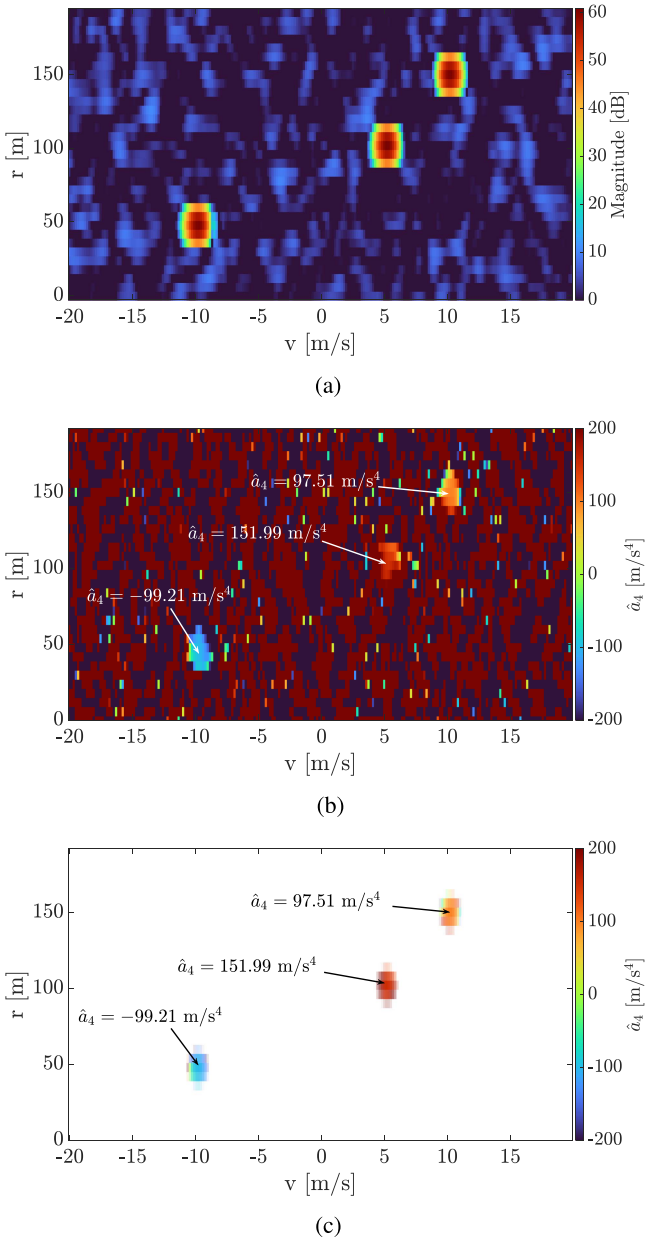

Fig. 4. Representative example of the snap estimation. (a) RV map of the three simulated targets. (b) Estimated snap distribution without saturation. (c) Estimated snap distribution with saturation.

in a low-power area. The processing is always done for the whole RV map, but the focus is on the strongest scatterers only for aesthetic reasons.

In Fig. 4(c), the targets' snap is shown, and the deviation between the set values and the estimated ones does not exceed 2.5%. The values were read at the maximum point of the RV map for a given target. The same procedure is used in the further analysis presented in this article. The estimation process took 0.17 s.

Let us analyze a single-target scenario to present the decomposition algorithm described by Algorithm 1. To do so, the simulated target at the initial range $R_0 = 100$ m had a velocity $V = 5$ m/s, acceleration $A = 0.5$ m/s^2, jerk $J = 20$ m/s^3, and

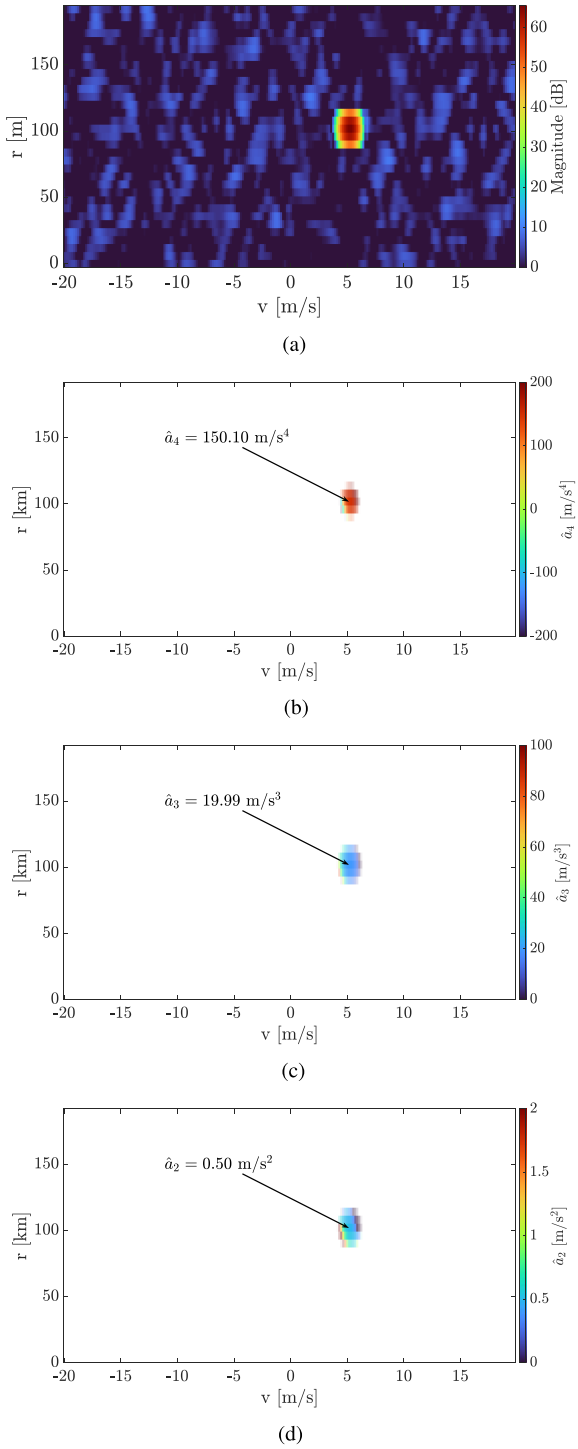

Fig. 5. Single-target simulation results—high-order kinematic parameter decomposition. (a) RV map of the simulated target. (b) Estimated snap. (c) Estimated jerk. (d) Estimated acceleration.

snap $S = 150$ m/s^4 (see Target 1 in Table I). The outcomes of target signal decomposition are shown in Fig. 5.

The target echo was successfully decomposed with good accuracy. Each estimate has a negligible error, which does not affect the general outcome. An additional analysis comprising only the acceleration estimation was conducted to prove that the higher order terms matter. If the jerk and snap are present in the signal and they are not removed (the signal is not demodulated according to Algorithm 1), the estimated acceleration was assessed as $\hat{a}_2 = 0.42$ m/s^2. The time for the entire signal decomposition was 4.15 s.

In the literature, estimation of target parameters in radars (active and passive) is tackled using the RFT approach [5], [6], [7], [27]. This precise yet extremely time-consuming technique has great potential; however, the real-time implementation for high-order kinematic parameter estimation with a dense grid is challenging. The main reason for the enormous computational burden in RFT stems from the nested loop for each parameter. For example, if one analyzes velocity, acceleration, jerk, and snap, and each parameter has a grid 101 points in size, the algorithm needs 101^4 iterations. The processing time was four weeks using the same computing machine as in the previous case and the MATLAB implementation. Although the result was precise, the RFT's usefulness in real-life applications is questionable. Certainly, the processing can be performed using more efficient implementation and graphic processing units, but still, real-time processing is infeasible, notably for a dense grid. Similar outcomes in terms of processing time were obtained for the method based on modulating the reference signal by factors related to high-order kinematic parameters [9], [14]. The processing time reaches several weeks for parameter sets of the same size (using MATLAB implementation). The next subsection compares the proposed method and two techniques from the literature in terms of efficiency.

B. Numerical Stability Assessment and Performance Analysis

As mentioned, a dense estimation of parameters using the RFT and through modulating the reference signal has a tangible processing time. The number of iterations of these methods was narrowed down so that the comparison could be performed in a reasonable time; namely, the results of 10 realizations were averaged to perform the processing in a suitable time. The simulated target at the range of $R = 100$ m was illuminated for 0.25 s with a signal at the carrier frequency of $f_c = 3.44$ GHz and with 50 MHz of bandwidth (the simulation assumed a noise signal imitating the OFDM waveform). Its kinematic parameters were as follows: $a_2 = 0.5$ m/s^2, $a_3 = 10$ m/s^3, $a_4 = 50$ m/s^4. The echo signal was 40 dB weaker than the reference one. Additionally, the surveillance signal (reflected from the target) was disturbed by additive white Gaussian noise of different values giving SNR $= \{-30, -20, -10, 0, 10, 20\}$ dB. Comprising the integration gain (49) equal to $G_i = 30.97$ dB, the SNR for the assumed simulation parameters is SNR $= \{0.97, 10.97, 20.97, 30.97, 40.97, 50.97\}$ dB. The results are shown in Fig. 6.

In line with expectations, the proposed method has higher errors than state-of-the-art methods based on (quasi) maximum likelihood estimation. However, the error does not matter for higher SNRs, as assumed at the beginning of this article. All techniques exhibit a rapid drop of the error for SNR greater than 10 dB; depending on the techniques, the ratio is more or less

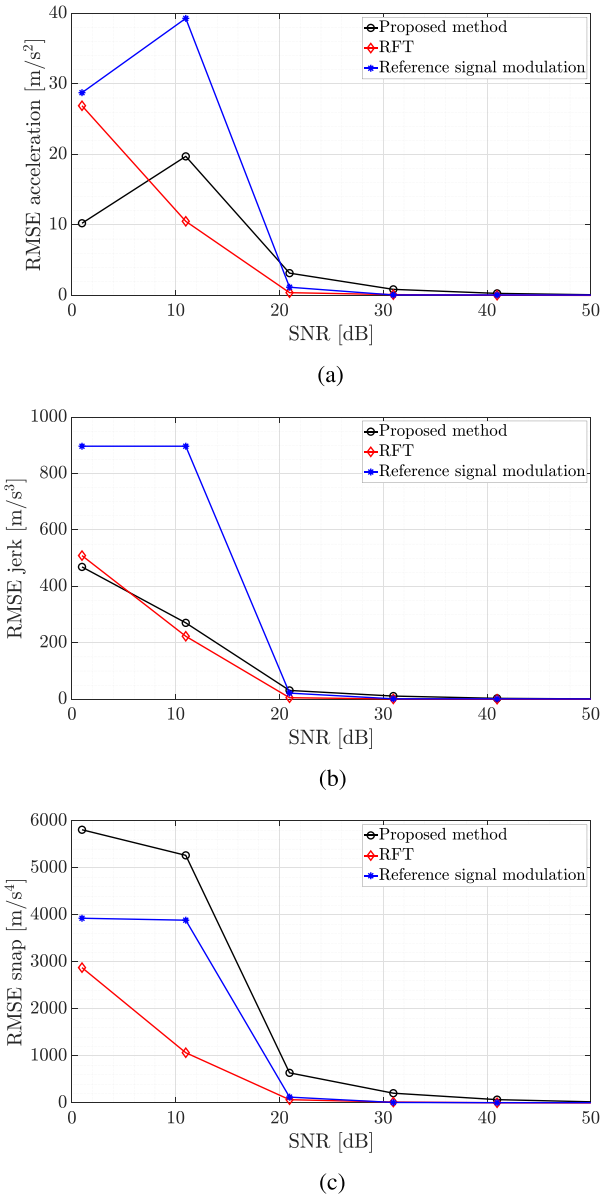

Fig. 6. Comparison of RMSE for the proposed and state-of-the-art methods. (a) RMSE for acceleration estimate. (b) RMSE for snap estimate. (c) RMSE for jerk estimate.

dynamic. Nevertheless, the overall outcomes were expected. The reference techniques use iterative modulation of the reference signal ([9]) or range profiles ([5], [6], [7], [27]) for finding the maximum of matched filtering, which gave more precise outcomes. Practical utilization of these techniques is challenging when simultaneously reducing the computational burden. As shown within the statistical analysis, the proposed method has a slightly worse precision; however, the outcome is obtained after much less than a second instead of days or weeks (for a very dense grid). Also, the highest error is obtained for snap. This error certainly affects the lower order estimates; however, its influence is not crucial as it depends on time in the fourth power. The error of the proposed method drops for snap and acceleration and can be neglected (or tuned if required) in practical scenarios,

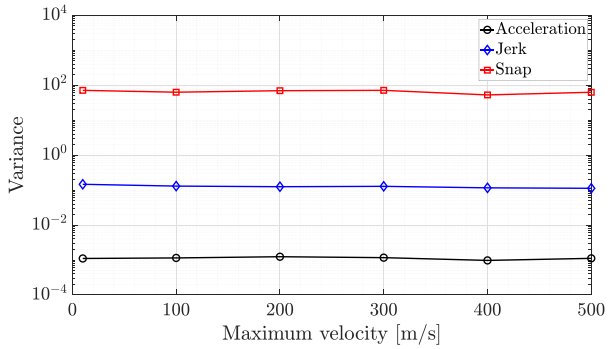

Fig. 7. Acceleration, jerk, and snap variance for the proposed method for different velocity ranges.

which is shown in the further part of this work. The result, although suboptimal, may serve as an initial condition for more precise but computationally demanding algorithms. Narrowing the set of values where the target kinematic parameters are estimated is crucial for accelerating the processing pipeline.

The outcomes impose limitations on the proposed method and entail constraints in leveraging it in real systems. As shown in Fig. 6, the proposed method stabilizes for a relatively high SNR (although SNR greater than 10 dB is a typical threshold for target detection). A natural application of the proposed method is short-range target detection, which is notably attractive for urban areas where typically a dense coverage of manifold low-power transmitters (for mobile communication) allows for commensal utilization of signals of opportunity.

C. Sensitivity to Velocity Axis Range

Although the proposed technique is nonparametric, one can wonder whether the velocity axis extension may improve the results. The Doppler axis range is related to the K parameter in (14) as it explicitly forces the slow-time dimension and defines the maximum target velocity in classical passive radar processing. To validate the influence of K on the proposed method, let us analyze the variance of acceleration, jerk, and snap estimates of the simulated target with parameters described in Section V-B for SNR $= 20.97$ dB (after integration). This value was chosen from the results in Fig. 6 as the proposed method's error rapidly drops, showing its usefulness but still with a small error. The experiment's aim was to verify whether the variance of this error could be suppressed by extending the analyzed velocity range. The outcomes for 100 Monte-Carlo simulations are illustrated in Fig. 7.

The results show no relationship between the estimation quality and the velocity axis size. The conclusion is consistent with the expectations because the proposed method is based on the Fourier transform. In the case of classical spectral analysis, a larger number of samples analyzed can improve the resolution of the transform and reduce the noise variance. When a signal is sampled according to Nyquist's theory, the Fourier transform can correctly determine its frequency. Also, the noise variance, which is expected to decrease when increasing the FFT size, does not affect the results in the analyzed case. This is due to the

fact that the SNR of the signal is high ($\sim$ 21 dB), so noise is not dominant. To sum up, the proposed method does not depend on the K parameter.

VI. Discussion

A. Signal Model Considerations

This research used the fourth-order polynomial for the Doppler shift modeling. There are two main reasons for this assumption.

1) *Influence of higher order parameters:* Usually, the polynomial defines kinematic parameters because such a representation is reasonable and convenient yet not far from reality. Nevertheless, the higher the order of the polynomial, the higher the power of t in the exponent that defines the surveillance signal. Since t is typically less than 1, increasing the exponent causes a significant reduction in the contribution of higher order kinematic components to the signal echo. The influence of higher order terms is usually neglected as they are too small to be reliably detected. Therefore, most of the existing methods deal with the kinematic model of the 4th-order maximum. The authors have not found any research where the kinematic parameters were considered for the order higher than 4 as they do not significantly improve radar signal processing (e.g., tracking).
2) *Numerical stability:* Higher order terms require a lot of discrete computations. In the simplest case, the Nth-order polynomial needs Nth-order derivative to estimate phase parameters (assuming its polynomial representation). For obvious reasons, one cannot compute the derivatives directly as the noise is too large in practice to efficiently compute the kinematic parameters. Therefore, one needs to perform additional processing steps. The presented approach needs, e.g., inverse matrices, to get the linear system solution. All of these operations introduce additional numerical errors resulting from a finite resolution of computers. All those small numerical errors accumulate, leading to large errors in the final estimate. The experiments that were conducted exhibited errors for the fourth-order polynomial model, which can be seen in Fig. 6(c). Increasing the polynomial order yields large numerical instabilities.

As mentioned, from the theoretical point of view, the proposed method can be extended to any polynomial order. However, the cost of numerical instabilities increases, and the benefits from the perspective of radar systems are too small to make the proposed method worth further extension.

B. Computational Complexity Analysis

Let us analyze the computational complexity of the proposed method. Equation (14) consists of signal correlation with the complexity of $\mathcal{O}(KL)$, where $L = T_b \cdot f_s$ is the number of range bins and K is the number of slow-time indices (equivalently the FFT size). In fact, the correlation can be done using the FFT formula, but this aspect is not considered herein. The second factor is the complexity of L Fourier transforms, each of the complexity $\mathcal{O}(K \log_2 K)$. The final computational cost is the sum of these factors, namely

$$\mathcal{C} = \mathcal{O}(KL) + \mathcal{O}\left(LK \log_2 K\right). \tag{50}$$

TABLE II
Computational Complexity Comparison; K – the Number of Slow-Time Points and the FFT Size, T_b – Signal Block Length, $L = T_b \cdot f_s$ – the Number of Range Bins, R_x, V_x, A_x, J_x, S_x – Discrete Sets of the Analyzed Parameters: Range, Velocity, Acceleration, Jerk, Snap, Respectively

Method	Computational complexity
Proposed method	$\mathcal{O}\left(LK \log_2 K\right)$
RFT	$\mathcal{O}\left(R_x, V_x, A_x, J_x, S_x K\right)$
Reference signal modulation	$\mathcal{O}\left(A_x, J_x, S_x KL\right)$+$\mathcal{O}\left(LK \log_2 K\right)$

To estimate high-order kinematic parameters using the proposed technique, one must always compute eleven RV maps with different windows and solve the same linear system, as described in Section III. These operations do not ultimately affect the computational cost given as (50). However, the range compression is computed only once. The most important part of the proposed technique is carried out on the signal after range compression, which is already computed in passive radar for the estimation of the bistatic range of targets. Therefore, a method similar to that presented in [2] was adopted, where range compression is not considered in the computational complexity analysis. This methodology reflects the actual computational load, considering a practical solution to the problem. The computational complexity of all considered methods in the Landau notation is listed in Table II.The proposed method's complexity results from the FFT cost along the slow-time dimension $\mathcal{O}(LK \log_2 K)$. In the RFT (where the range compression computational cost is neglected), the complexity is the product of the size of each parameter set [2]. For the reference signal modulation method, the computational complexity is also high, but compared to the RFT technique, the sets of range and velocity of the target are not considered. Instead, the FFT size has to be taken into account. From Table II, it is clear that the proposed technique is computationally efficient as the estimated parameters are not fixed to the grid, whose size can change (and can be large in practice).

Let us analyze the results in Fig. 8 to visualize the difference in the computational burden of the analyzed methods. The parameter K (number of slow-time samples/FFT size) was changed alongside the size of parameter sets. It was assumed that N_x is the size of each set defining range, velocity, acceleration, jerk, and snap. The results for three different values $N_x = 10, 100$, and 1000 were analyzed and compared according to the complexity from Table II. Also, the length of the signal block (number of range bins—the number of samples after range compression of each signal block) was analyzed. The corresponding results for $L = 100$ and $L = 1000$ are delineated in Fig. 8(a) and (b), respectively. The proposed method surpasses the state-of-the-art techniques of several orders of magnitude, even for the lowest N_x. The same observation is apparent in processing time reduction, which is presented in the next section.

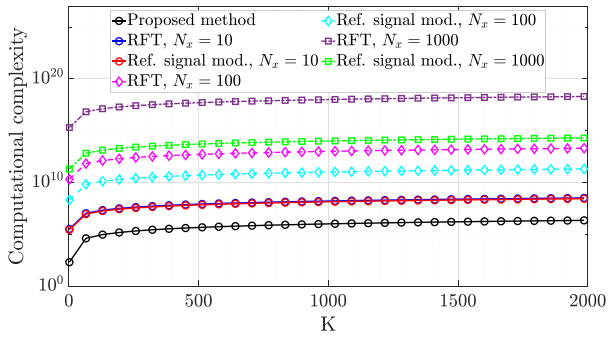

(a)

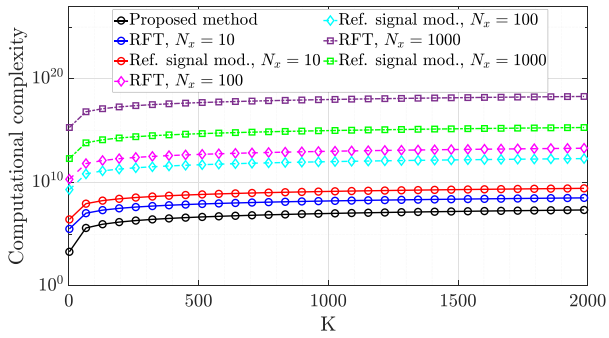

(b)

Fig. 8. Comparison of the computational complexity for different signal lengths and size of parameter sets. (a) Computational complexity comparison $L = 100$. (b) Computational complexity comparison $L = 1000$.

VII. Real-Life Data Analysis

As an illustrative example of the method's performance, a real-life 5G-based passive radar signal was processed. The details regarding the measurement trials were presented in [28]. In short, the experiment was carried out at the campus of the Łódź University of Technology, Poland, and its goal was to detect a drone using passive radar. The illuminator of opportunity was a 5G cooperative network whose signal was sampled with a rate of $f_s = 50$ MSa/s. The system carrier frequency was $f_c = 3.44$ GHz, and the maximum bandwidth was $B = 38.16$ MHz, which results in a maximum bistatic range resolution of approximately 7.8 m. The network works with the time division duplex (TDD) mode. Since the 5G standard assumes a content-dependent transmission, there was a need to force a downlink transmission by downloading a massive file using a mobile phone. This ensured a full utilization of time and frequency resources and the continuous illumination of a drone. The drone used in the experiment and the measurement scenario is shown in Fig. 9.

The recorded signal was processed after the trials. A selected signal part was extracted, and the experiments using the considered methods were carried out. The RV map based on which the high-order kinematic parameter estimation was performed is shown in Fig. 10. The outcome was obtained for the integration time $T_i = 0.25$ s. The drone echo is apparent at $R = 65.95$ m, and its velocity is computed as $V = 6.82$ m/s. Apart from the drone's main body reflection, characteristic so-called flashes (propellers' flickering) resulting from rotating blades can be

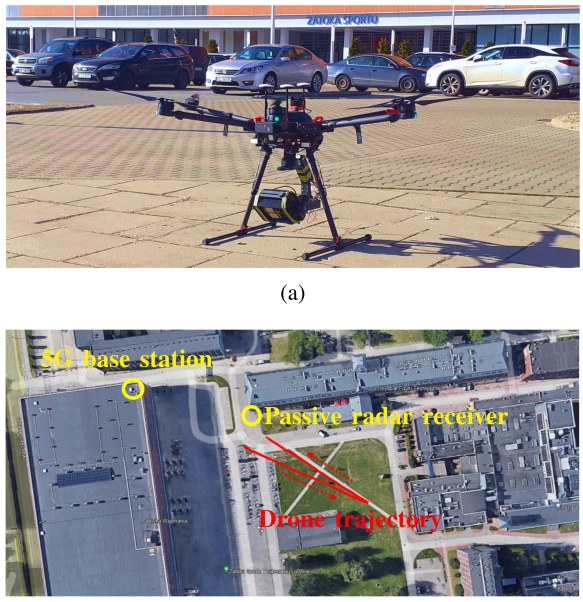

(a)

(b)

Fig. 9. Measurement scenario. Cooperative drone and the measurement scenario. (a) Drone—a cooperative target. (b) Experiment geometry.

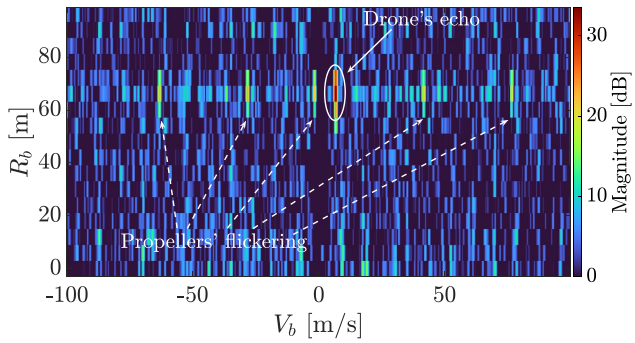

Fig. 10. RV map for the real-life 5G-based passive radar measurement.

seen. They are at the same range as the main target, but their velocities are periodically distributed over the velocity axis. The SNR of the echo signal was relatively high, as the statistical analysis showed all the methods' performance for small noise, and this experiment's goal was to compare the estimated values and the reduction of processing time (the estimated SNR was approximately 33.5 dB). All of these parameters are compared for the proposed method and the reference techniques.

Although the GPS recorder was mounted on the drone, its acquisition rate was 1 s; thus, the precise values of movement parameters cannot be assessed. Notably, for the assumed integration time, the high-order kinematic parameters can only be calculated as the derivatives of the velocity discretized with a lower frequency than the observation. Therefore, the results obtained using the maximum-likelihood estimators (the reference methods) are treated as the ground-truth values.

The estimation procedure was as follows.

1) The proposed method was applied to roughly assess the space of parameters as their precise values were unknown.

TABLE III
RESULTS OF THE ESTIMATION PROCESS FOR THE REAL-LIFE SIGNAL

Method	Parameter	Value
Proposed method	$\hat{a}_2(t,\omega)$ [m/s^2]	1.92
	$\hat{a}_3(t,\omega)$ [m/s^3]	-8.10
	$\hat{a}_4(t,\omega)$ [m/s^4]	-493.54
	t [s]	7.64
RFT	$\hat{a}_2(t,\omega)$ [m/s^2]	1.80
	$\hat{a}_3(t,\omega)$ [m/s^3]	-8.40
	$\hat{a}_4(t,\omega)$ [m/s^4]	-400.00
	t [s]	$5.88 \cdot 10^3$
Ref. signal mod.	$\hat{a}_2(t,\omega)$ [m/s^2]	2.00
	$\hat{a}_3(t,\omega)$ [m/s^3]	-8.00
	$\hat{a}_4(t,\omega)$ [m/s^4]	-480.00
	t [s]	$2.58 \cdot 10^4$

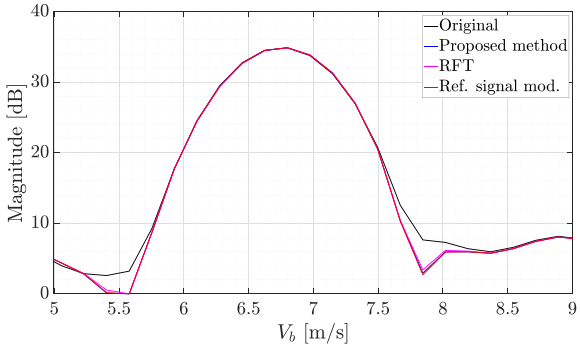

Fig. 11. RV map cross sections before and after removing high-order kinematic parameters from the surveillance signal.

2) Using each of the initial estimates $\hat{a}_2(t,\omega)$, $\hat{a}_3(t,\omega)$, and $\hat{a}_4(t,\omega)$, the discrete set was created with a central point given by values obtained using the proposed method. Each set had 11 points.
3) A fine-tuning of the parameters was performed using two reference methods.
4) A final validation was based on comparing the estimated values and the processing time.

The results are shown in Table III .

The outcomes show a cohesion of the estimated values. Simulations showed the RFT technique as the most accurate; however, the other methods gave similar results. The most important factor is the processing time, which can be reduced using the proposed method. The time reduction is enormous. Although the proposed method is less efficient (it is supposed that the state-of-the-art algorithms are more precise), it gave a starting point for iterative and accurate methods. Without it, the whole computation time for the reference techniques would be greater. The surveillance signal was demodulated using estimated values obtained using each method to assess the quality of the estimates. Next, the RV map was computed, and their cross sections for the range cell containing the drone's echo are plotted in Fig. 11. As can be seen, removing high-order kinematic parameters allowed for narrowing the peak. There is also a negligible discrepancy between the results for different estimation methods.

Two reference methods were experimentally validated to express the impact of the initial estimation of the kinetic parameters (which provides a point around which precise estimation can be made). It was assumed that the point estimated using the proposed method is unknown. Therefore, acceleration was looked for in the range $[-10, 10]$ m/s^2, jerk in $[-100, 100]$ m/s^3, and snap in $[-1000, 1000]$ m/s^4. Each set had 11 points. Due to the sparse grid, the estimated parameters for both methods were as follows: $\hat{a}_2(t,\omega) = 2$ m/s^2, $\hat{a}_2(t,\omega) = 0$ m/s^3, and $\hat{a}_2(t,\omega) = -400$ m/s^4. Apart from the less precise estimate, the processing time (as shown in Table III) was extremely long. Moreover, increasing the number of points in each set to improve the precision will further extend processing time.

VIII. CONCLUSION

This article has addressed three specific objectives. First, the mathematical derivations of passive radar signal processing have been provided. As a result, the link between theoretical (CAF) and practical (Woodward's approximation using the Zak transform) considerations was proposed. The article presented a compact analytical formulation of how passive radar signals are processed in practice. Second, the simple yet numerically efficient approach to rough high-order target kinematic parameter estimation in passive radar was proposed. In contrast to classical methods in the literature, the proposed one is gridless and does not require a starting point when looking for the estimates. Compared to existing techniques, the processing time was reduced by four orders of magnitude. Of course, the method is less precise; however, as shown in real-life experiments, it can serve as an initial estimate for further fine-tuning methods. Due to the requirement of a relatively high SNR (> 10 dB), the method can be primarily used in short-range applications or whenever the target echo satisfies the SNR condition. Moreover, the presented approach is suitable for further extension for higher order degrees, notwithstanding the numerical instabilities associated with higher order terms. The limitations assumed in this article stem from its limited scope. Nevertheless, differentiating (35) according to (37) enables the extension of the proposed method. Last but not least, the method was used for real-life experiments using a 5G-based passive radar for drone detection. The outcomes confirmed the proposed method's efficacy and meaningful numerical performance. Future developments of the presented technique focus on real-time implementation using highly efficient platforms such as graphics processing units (GPUs). Parallel processing should enable the extraction of target kinematic parameters within integration time, a crucial requirement for real-world applications.

APPENDIX

Let us recall the definition of the passive radar processing (14)

$$\mathcal{Z}^h(t,\omega) = \sum_{k=-\frac{K}{2}}^{\frac{K}{2}-1} \int_0^{T_b} x_s(\tau+kT) x_r^*(\tau+kT-t)\, h(kT-t) \times e^{-j\omega(kT-t)} \mathrm{d}\tau. \quad (51)$$

To estimate t, one has to compute the derivative of (51) with respect to ω

$$\frac{\partial \mathcal{Z}^h(t,\omega)}{\partial \omega} = \frac{\partial}{\partial \omega} \sum_{k=-\frac{K}{2}}^{\frac{K}{2}-1} \int_0^{T_b} x_s(\tau + kT) x_r^*(\tau + kT - t) \times h(kT - t) e^{-j\omega(kT-t)} \mathrm{d}\tau. \tag{52}$$

Let us compare the right-hand side of (52) to 0

$$\frac{\partial}{\partial \omega} \sum_{k=-\frac{K}{2}}^{\frac{K}{2}-1} \int_0^{T_b} x_s(\tau + kT) x_r^*(\tau + kT - t) \times h(kT - t) e^{-j\omega(kT-t)} \cdot \mathrm{d}\tau = 0. \tag{53}$$

Next, one has

$$-j(kT - t) \sum_{k=-\frac{K}{2}}^{\frac{K}{2}-1} \int_0^{T_b} x_s(\tau + kT) x_r^*(\tau + kT - t) \times h(kT - t) e^{-j\omega(kT-t)} \cdot \mathrm{d}\tau = 0. \tag{54}$$

Since $kT\mathcal{Z}^h(t,\omega) = \mathcal{Z}^{\mathcal{J}h}(t,\omega)$, we can write

$$\mathcal{Z}^{\mathcal{J}h}(t,\omega) = t\mathcal{Z}^h(t,\omega) \tag{55}$$

thus, the time delay estimator reads as

$$\hat{t}(t,\omega) = \frac{\mathcal{Z}^{\mathcal{J}h}(t,\omega)}{\mathcal{Z}^h(t,\omega)}. \tag{56}$$

ACKNOWLEDGMENT

The authors would like to thank Prof. P. Samczyński, Prof. T. Zieliński, Dr. J. Wszołek, Mr. M. Płotka, and Mr. R. Maksymiuk for their support in the measurement campaign and the team from the Łódź University of Technology for providing the facility for trials.

REFERENCES

[1] H. D. Griffiths and C. J. Baker. *An Introduction to Passive Radar*. Norwood, MA, USA: Artech House, 2017.

[2] X. Li, G. Cui, W. Yi, and L. Kong, "Radar maneuvering target detection and motion parameter estimation based on TRT-SGRFT," *Signal Process.*, vol. 133, pp. 107–116, 2017.

[3] J. Xu, X.-G. Xia, S.-B. Peng, J. Yu, Y.-N. Peng, and L.-C. Qian, "Radar maneuvering target motion estimation based on generalized Radon-Fourier transform," *IEEE Trans. Signal Process.*, vol. 60, no. 12, pp. 6190–6201, Dec. 2012.

[4] H. Lin, C. Zeng, H. Zhang, and G. Jiang, "Radar maneuvering target motion parameter estimation based on hough transform and polynomial Chirplet transform," *IEEE Access*, vol. 9, pp. 35178–35195, 2021.

[5] J. Xu, J. Yu, Y.-N. Peng, and X.-G. Xia, "Radon-Fourier transform for radar target detection, I: Generalized doppler filter bank," *IEEE Trans. Aerosp. Electron. Syst.*, vol. 47, no. 2, pp. 1186–1202, Apr. 2011.

[6] J. Xu, J. Yu, Y.-N. Peng, and X.-G. Xia, "Radon-Fourier transform for radar target detection (II): Blind speed sidelobe suppression," *IEEE Trans. Aerosp. Electron. Syst.*, vol. 47, no. 4, pp. 2473–2489, Oct. 2011.

[7] J. Yu, J. Xu, Y.-N. Peng, and X.-G. Xia, "Radon-Fourier transform for radar target detection (III): Optimality and fast implementations," *IEEE Trans. Aerosp. Electron. Syst.*, vol. 48, no. 2, pp. 991–1004, Apr. 2012.

[8] X. Gao, H. Zhang, and T. Dang, "Radar detection and fast motion parameter estimation for complex manoeuvering targets at high speed and acceleration," *IET Radar, Sonar Navigation*, vol. 16, no. 12, pp. 1977–1996, 2022.

[9] M. Malanowski, "Detection and parameter estimation of manoeuvring targets with passive bistatic radar," *IET Radar, Sonar Navigation*, vol. 6, no. 8, pp. 739–745, Oct. 2012.

[10] K. Abratkiewicz, M. Malanowski, and Z. Gajo, "Target acceleration estimation in active and passive radars," *IEEE J. Sel. Topics Appl. Earth Observ. Remote Sens.*, vol. 16, pp. 9193–9206, 2023.

[11] P. Huang, G. Liao, Z. Yang, X.-G. Xia, J.-T. Ma, and J. Ma, "Long-time coherent integration for weak maneuvering target detection and high-order motion parameter estimation based on keystone transform," *IEEE Trans. Signal Process.*, vol. 64, no. 15, pp. 4013–4026, Aug. 2016.

[12] Q. Liu, J. Guo, Z. Liang, and T. Long, "Motion parameter estimation and HRRP construction for high-speed weak targets based on modified GRFT for synthetic-wideband radar with PRF jittering," *IEEE Sensors J.*, vol. 21, no. 20, pp. 23234–23244, Oct. 2021.

[13] X. Chen, Y. Huang, N. Liu, J. Guan, and Y. He, "Radon-fractional ambiguity function-based detection method of low-observable maneuvering target," *IEEE Trans. Aerosp. Electron. Syst.*, vol. 51, no. 2, pp. 815–833, Apr. 2015.

[14] Z. Solatzadeh and A. Zaimbashi, "Accelerating target detection in passive radar sensors: Delay-Doppler-acceleration estimation," *IEEE Sensors J.*, vol. 18, no. 13, pp. 5445–5454, Jul. 2018.

[15] J. Palmer, S. Palumbo, A. Summers, D. Merrett, S. Searle, and S. Howard, "An overview of an illuminator of opportunity passive radar research project and its signal processing research directions," *Digit. Signal Process.*, vol. 21, no. 5, pp. 593–599, 2011.

[16] C. Moscardini, D. Petri, A. Capria, M. Conti, M. Martorella, and F. Berizzi, "Batches algorithm for passive radar: A theoretical analysis," *IEEE Trans. Aerosp. Electron. Syst.*, vol. 51, no. 2, pp. 1475–1487, Apr. 2015.

[17] C. Baylis, L. Cohen, D. Eustice, and R. Marks, "Myths concerning Woodward's ambiguity function: Analysis and resolution," *IEEE Trans. Aerosp. Electron. Syst.*, vol. 52, no. 6, pp. 2886–2895, Dec. 2016.

[18] D. Eustice, C. Baylis, and R. J. Marks, "Woodward's ambiguity function: From foundations to applications," in *Proc. Texas Symp. Wireless Microw. Circuits Syst.*, 2015, pp. 1–17.

[19] J. Zak, "Finite translations in solid-state physics," *Phys. Rev. Lett.*, vol. 19, pp. 1385–1387, Dec. 1967.

[20] J. Zak, "Dynamics of electrons in solids in external fields," *Phys. Rev.*, vol. 168, pp. 686–695, Apr. 1968.

[21] A. K. Brodzik, "Signal extrapolation in the real Zak space," *IEEE Trans. Signal Process.*, vol. 50, no. 8, pp. 1957–1964, Aug. 2002.

[22] V. S. Bhat, G. Harshavardhan, and A. Chockalingam, "Input-output relation and performance of RIS-Aided OTFS with fractional delay-doppler," *IEEE Commun. Lett.*, vol. 27, no. 1, pp. 337–341, Jan. 2023.

[23] I. Gladkova, "Zak transform and a new approach to waveform design," *IEEE Trans. Aerosp. Electron. Syst.*, vol. 37, no. 4, pp. 1458–1464, Oct. 2001.

[24] I. Gladkova, "Design of frequency modulated waveforms via the Zak transform," *IEEE Trans. Aerosp. Electron. Syst.*, vol. 40, no. 1, pp. 355–359, Jan. 2004.

[25] P. M. Woodward, *Probability and Information Theory, With Applications to Radar: International Series of Monographs on Electronics and Instrumentation*, vol. 3. New York, NY, USA: Elsevier, 2014.

[26] D.-H. Pham and S. Meignen, "High-order synchrosqueezing transform for multicomponent signals analysis–with an application to gravitational-wave signal," *IEEE Trans. Signal Process.*, vol. 65, no. 12, pp. 3168–3178, Jun. 2017.

[27] Y. Yin, S. Zhang, F. Wu, Z. Zong, and W. Zhang, "Passive radar detection with DVB-T signals," in *Proc. CIE Int. Conf. Radar*, 2016, pp. 1–5.

[28] R. Maksymiuk, K. Abratkiewicz, P. Samczyński, and M. Płotka, "Rényi entropy-based adaptive integration method for 5G-based passive radar drone detection," *Remote Sens.*, vol. 14, no. 23, 2022, Art. no. 6146.